Acta Geochim (2019) 38(3):414–429
https://doi.org/10.1007/s11631-019-00322-4

ORIGINAL ARTICLE

Trace element partitioning between amphibole and hydrous silicate glasses at 0.6–2.6 GPa

Bo Zhang[1,2] · Xianxu Hu[3] · Peng Li[4] · Qizhe Tang[1,2] · Wenge Zhou[1]

Received: 12 December 2018 / Revised: 24 January 2019 / Accepted: 19 February 2019 / Published online: 1 March 2019

Abstract Partitioning behavior between amphibole and silicate glass of thirty-three minor and trace elements (Sc, Ti, V, Cr, Co, Rb, Sr, P, Y, Zr, Nb, Cs, Ba, K, La, Ce, Pr, Nd, Sm, Eu, Gd, Tb, Dy, Ho, Er, Tm, Yb, Lu, Hf, Ta, Pb, Th, and U) have been determined experimentally. Products of crystallization of hydrous basalt melts from 0.6 GPa/860 °C up to 2.6 GPa/970 °C were obtained in a multi-anvil apparatus. Major and trace element compositions of amphibole and glass were determined with a combination of electron microprobe and laser ablation inductively coupled plasma mass spectrometry. The main mineral phase is calcic amphibole, and the coexisting glass compositions are tonalite, granodiorite, and granite. The compatibility of rare earth elements increase at 915 °C and then decrease at 970 °C, but the compatibility of most of these elements shows a continued, significant increase with increasing pressure. For high-field strength elements, large ion lithophile elements, actinide compatibility decrease with increasing temperature or pressure, but transition metals show a continued increase in compatibility within the temperature–pressure conditions. From mathematical and graphical fitting, we determined best-fit values for the ideal ionic radius (r_0, 1.01–1.04 Å), the strain-free partition coefficient (D_0, 1.18–1.58), and apparent Young's modulus (E, 142–370 GPa) for the M4 site in amphibole according to the lattice strain model. The D_0^{M4} for rare earth elements rises at 915 °C and then drops at 970 °C at 0.6 GPa. However, the D_0^{M4} values are positively proportional to the pressure for rare earth elements in the amphibole-glass pairs at 0.6–2.6 GPa and 970 °C. Furthermore, the derived best-fit values for r_0^{M4} and E^{M4} are almost constant and trend to increase with rising temperature and pressure, respectively. The partition coefficient is distinctly different for different melt compositions. The rare earth elements become more enriched in amphibole if the quenched glass is granodiorite or granite compared to the tonalitic glasses.

Keywords Amphibole · Silicate glass · Trace elements · Partition coefficients · Lattice strain model

1 Introduction

The partition coefficient describes the distribution of an element between a mineral and melt. The Nernst partition coefficient is defined as D_i= (concentration of element i in mineral)/(concentration of element i in melt). One could obtain quantitative understandings on igneous evolution by estimating the parental melt compositions with relevant D values between minerals and melts (Lundstrom et al. 2000; Landwehr et al. 2001; Frei et al. 2009; Severs et al. 2009; Parker et al. 2010; Chang et al. 2016; Cui et al. 2017). However, due to the effects of temperature, pressure and composition, mineral/melt D values show enormous variations (Blundy and Wood 2003; Adam and Green 2006; Severs et al. 2009; Sun 2018).

✉ Wenge Zhou
zhouwenge@vip.gyig.ac.cn

[1] Key Laboratory for High Temperature and High Pressure Study of the Earth's Interior, Institute of Geochemistry, Chinese Academy of Sciences, Guiyang 550081, China

[2] University of Chinese Academy of Sciences, Beijing 100049, China

[3] Guizhou University of Finance and Economics, Guiyang 550025, China

[4] Guizhou Institute of Technology, Guiyang 550003, China

Most of the partition coefficient studies focus on minerals and silicate melts. These minerals include amphibole (Adam and Green 2006; Tiepolo et al. 2007; Nandedkar et al. 2016; Shimizu et al. 2017), clinopyroxene (Adam and Green 2006; Hill et al. 2011; Sun and Liang 2012; Mollo et al. 2017), orthopyroxene (Adam and Green 2006; Frei et al. 2009; Parker et al. 2010; Sun and Liang 2013a), garnet (Adam and Green 2006; Draper and Westrenen 2007; Sun and Liang 2013b), plagioclase (Severs et al. 2009; Sun et al. 2017), olivine (Adam and Green 2006; Sun and Liang 2013b; Stead et al. 2017), and some infrequent crystals such as rutile (Klemme et al. 2005; Xiong et al. 2005), and apatite (Prowatke and Klemme 2006). Additionally, few published literatures showed the distribution of trace elements between amphibole, clinopyroxene, garnet, apatite and carbonatite melts (Sweeney et al. 1992, 1995; Blundy and Dalton 2000; Klemme and Dalpé 2003; Dasgupta et al. 2009).

Different techniques have been used to determine partition coefficient of trace elements between minerals and melts. Several studies have measured trace elements in minerals and surrounding glassy matrix. The first kind of studies measured the contents of trace elements in minerals and the surrounding glassy matrix (Arzamastsev et al. 2009; Severs et al. 2009; Olin and Wolff 2010; Mollo et al. 2017). Moreover, the melt inclusion-mineral (MIM) technique was introduced to determine partitioning behavior of elements (Thomas et al. 2002; Zajacz and Halter 2007; Severs et al. 2009; Nardi et al. 2013). Finally, minerals and melts from experimental products were used to determine the partitioning of trace elements (Blundy and Dalton 2000; Dalpé and Baker 2000; Adam and Green 2006; Frei et al. 2009; Parker et al. 2010; Hill et al. 2011). These methods have been used to determine partition coefficients for the trace elements in various compositions of minerals and co-existing melts. Generally, mineral phases-melt systems with many minerals were investigated rather than a single mineral-melt system in most of the previous studies (Adam and Green 2006; Arzamastsev et al. 2009; Severs et al. 2009; Wan et al. 2009). For example, Adam and Green (2006) discussed the partition coefficients of trace elements between amphibole, clinopyroxene, orthopyroxene, garnet, olivine and coexisting melt in the same system. Furthermore, it is well known that partition coefficient depends on the chemical compositions of mineral and melt, on pressure and temperature and on H_2O-content of the melt (Blundy and Wood 2003; Adam and Green 2006; Severs et al. 2009; Parker et al. 2010; Hill et al. 2011; Sun et al. 2017).

In addition, a theoretical framework based on the lattice strain model (Brice 1975) was provided for trace element partitioning (Blundy and Wood 1994). So far, the theory has been applied successfully to trace element partitioning between clinopyroxene (Wood and Blundy 1997; Adam and Green 2006; Sun and Liang 2012), garnet (Draper and Westrenen 2007; Westrenen and Draper 2007; Sun and Liang 2013b), and amphibole (Adam and Green 2006; Tiepolo et al. 2007; Wan et al. 2009) and the coexisting melt with each other. These studies have shown that partition coefficients vary as a function of crystal and melt composition, pressure and temperature. The influence of melt composition and temperature on the distribution of trace elements has been studied abundantly (Klein et al. 1997; Tiepolo et al. 2000; Nandedkar et al. 2016; Shimizu et al. 2017; Sun 2018). However, the systematic study of the effect of pressure on the distribution of trace elements is relatively lacking.

Table 1 Bulk composition of sample 10084

Oxide	wt%	Element	ppm	Element	ppm	Element	ppm
SiO_2	47.80	Sc	15.70	Pr	10.5	Ta	6.40
Al_2O_3	14.13	Ti	14,880	Nd	39.7	Th	8.30
TiO_2	2.48	V	220	Sm	7.56	U	1.65
MgO	6.44	Cr	102	Eu	2.38		
Fe_2O_3	7.57	Rb	18.40	Gd	6.72		
FeO	3.53	Sr	1009	Tb	0.88		
MnO	0.16	Y	21.60	Dy	4.79		
CaO	8.40	Zr	265	Ho	0.81		
Na_2O	3.90	Nb	62.50	Er	1.94		
K_2O	1.26	Ba	789	Tm	0.25		
CO_2	0.02	K	10,455	Yb	1.29		
H_2O^+	3.33	La	44.79	Lu	0.19		
Total	99.02	Ce	88.18	Hf	6.70		

Sample number 10084 from Zhou et al. (1998)

Major- and trace-elements concentration are given in wt% and ppm, respectively

Table 2 Run conditions and phase compositions of amphibole and glass in experimental products

Run No.	10084-1		10084-2		10084-3		10084-4		10084-5		10084-6		10084-7	
T/°C	1460/860		1460/915		1460/970		1490/970		1515/970		1540/970		1570/970	
P/GPa	0.6		0.6		0.6		1.1		1.6		2.1		2.6	
Phase	Amp + Ab + Apa + Gl		Amp + Apa + Gl		Amp + Apa + Gl		Amp + Apa + Gl		Amp + Apa + Gl		Amp + Apa + Sp + Gl		Amp + Apa + Sp + Gl	
n	Amp (4)	Gl (4)	Amp (4)	Gl (4)	Amp (5)	Gl (7)	Amp (5)	Gl (4)	Amp (4)	Gl (4)	Amp (11)	Gl (6)	Amp (6)	Gl (4)
SiO_2 (wt%)	43 (3)	62 (3)	41 (2)	65.1 (8)	40.9 (7)	60.7 (6)	40.5 (9)	61.3 (3)	39.2 (5)	66.1 (6)	40 (1)	64.7 (8)	39.7 (3)	65.4 (9)
Al_2O_3	12 (3)	23 (2)	14.3 (8)	20.3 (4)	13.5 (4)	20.1 (2)	14.6 (5)	20.1 (3)	15.7 (7)	19.27 (9)	16.1 (8)	19.4 (1)	16 (1)	20.6 (4)
TiO_2	3.1 (8)	0.11 (6)	3.4 (3)	0.50 (4)	3.5 (4)	0.90 (6)	3.7 (4)	0.80 (8)	3.9 (1)	0.78 (3)	3.1 (5)	0.77 (5)	3.2 (4)	0.87 (8)
Cr_2O_3	0.14 (9)	0.08 (7)	0.05 (3)	0.04 (3)	0.2 (1)	0.09 (8)	0.04 (3)	0.02 (1)	0.04 (4)	0.02 (1)	0.08 (4)	0.1 (1)	0.06 (2)	0.03 (1)
MgO	11.4 (4)	0.04 (3)	10.3 (8)	0.4 (1)	10.9 (5)	1.3 (8)	11 (1)	0.7 (2)	8.6 (6)	0.57 (3)	10.2 (5)	0.72 (5)	9.5 (2)	0.45 (3)
NiO	0.02 (1)	0.02 (1)	0.03 (0)	0.01 (1)	0.02 (2)	0.02 (1)	0.01 (1)	0.01 (1)	0.02 (2)	0.03 (1)	0.04 (2)	0.01 (1)	0.02 (1)	0.03 (1)
FeO*	13 (1)	0.6 (2)	13.0 (8)	3.02 (3)	14.0 (7)	5.5 (2)	13.2 (8)	4.6 (9)	14.9 (4)	3.6 (1)	12 (1)	3.4 (1)	13 (2)	3.0 (2)
MnO	0.23 (8)	0.04 (3)	0.19 (2)	0.07 (2)	0.18 (5)	0.14 (4)	0.18 (1)	0.12 (3)	0.17 (2)	0.06 (2)	0.16 (6)	0.09 (1)	0.17 (3)	0.06 (2)
CaO	12 (3)	6 (2)	10.6 (9)	2.6 (2)	10.3 (2)	4.5 (2)	10.7 (3)	3.3 (1)	9.9 (2)	2.17 (2)	10 (1)	2.6 (2)	10.7 (3)	2.1 (2)
Na_2O	2.4 (7)	7 (2)	2.8 (1)	6.86 (3)	2.82 (7)	5.6 (2)	2.59 (8)	6.1 (2)	3.02 (4)	5.45 (5)	3.1 (1)	6.1 (2)	2.9 (2)	5.0 (1)
K_2O	1.1 (3)	1.3 (7)	1.4 (2)	1.5 (2)	1.0 (2)	1.33 (4)	1.7 (6)	2.9 (3)	1.9 (2)	1.92 (9)	1.9 (6)	2.1 (1)	1.7 (5)	2.4 (3)
Total	97.89	100	97.44	100	97.24	100	97.76	100	97.23	100	96.39	100	96.84	100

The totals of glass major element compositions are normalized to 100 wt%. 1460/860 indicates the melting temperature and crystallization temperature. *n* is the number of analyses for the corresponding phase. All the experiments are held 100 h at each run *T-P* conditions. Total Fe is given as FeO. The numbers in the parentheses are the 1σ error of the mean and reported as the least unit cited. For example, 43(3), 3.1(8), and 0.14(9) should be read as 43 ± 3 wt%, 3.1 ± 0.8 wt%, and 0.14 ± 0.09 wt%, respectively

Amp amphibole, *Apa* apatite, *Sp* spinel, *Ab* albite, *Gl* quenched glass

Table 3 Trace element data of experimental products for hydrous basalt

RUN No.	10084-1		10084-2		10084-3		10084-4	
Phase (*n*)	Amp (4)	Gl (4)	Amp (5)	Gl (6)	Amp (7)	Gl (4)	Amp (7)	Gl (5)
Sc	20.6 (0.9)	18.5 (0.2)	20.5 (1.5)	18.2 (2.9)	29.3 (4.9)	15.8 (5.8)	21.4 (1.6)	3.29 (1.21)
Ti	9441 (901)	8750 (485)	13462 (1093)	11,439 (1076)	20,913 (2200)	11,500 (401)	21,733 (1791)	5144 (403)
V	133 (10)	126 (6)	159 (15)	136 (35)	351 (57)	155 (62)	298 (23)	9.92 (0.87)
Cr	131 (26)	125 (9)	168 (17)	115 (39)	353 (50)	194 (59)	293 (29)	24 (13)
Rb	33.4 (2.3)	31.4 (2.3)	65.9 (5.0)	77.6 (6.1)	24.3 (1.9)	68.9 (5.8)	20.1 (1.8)	183.6 (7.6)
Sr	929 (80)	686 (48)	783 (38)	789 (76)	850 (94)	1072 (129)	761 (57)	1390 (51)
Y	15.9 (1.2)	11.4 (0.6)	47.7 (4.1)	23.3 (2.5)	23.6 (1.9)	21.6 (2.1)	21.4 (1.0)	14.7 (1.4)
Zr	162 (19)	139 (12)	229 (18)	252 (20)	187 (15)	284 (26)	142 (10)	356 (12)
Nb	36.4 (2.7)	33.9 (2.7)	53.2 (2.8)	48.7 (2.5)	56.4 (3.4)	69.4 (4.3)	49.3 (4.1)	84.0 (4.6)
Cs	3.12 (0.65)	2.09 (0.07)	5.57 (0.69)	6.67 (0.55)	1.96 (0.19)	5.43 (1.66)	1.46 (1.14)	15.3 (1.0)
Ba	479 (48)	409 (44)	586 (41)	600 (57)	416 (399)	780 (62)	389 (31)	1123 (34)
K	10,612 (1204)	9201 (297)	17,074 (1105)	18,317 (2404)	7885 (656)	15,386 (1333)	10,713 (1581)	33,763 (715)
La	15.7 (1.5)	68.2 (0.7)	42.5 (2.5)	69.2 (6.3)	27.2 (2.3)	57.4 (3.2)	24.6 (1.6)	76.3 (8.2)
Ce	45.6 (6.2)	121 (1)	84.8 (4.5)	114 (11)	59.8 (5.1)	102 (8)	57.7 (6.8)	127 (10)
Pr	7.88 (0.71)	12.2 (0.1)	9.39 (1.43)	11.3 (1.2)	7.92 (0.18)	11.3 (1.8)	7.44 (1.03)	12.1 (1.3)
Nd	39.1 (2.4)	45.4 (0.5)	40.7 (3.5)	38.7 (2.2)	35.1 (2.8)	42.2 (2.5)	34.9 (1.2)	39.8 (2.8)
Sm	4.60 (0.87)	4.10 (0.28)	8.76 (1.98)	6.61 (1.28)	8.56 (1.57)	7.59 (1.90)	7.25 (1.18)	7.55 (0.24)
Eu	1.70 (0.37)	1.45 (0.31)	2.20 (0.40)	1.59 (0.33)	2.78 (0.71)	2.20 (0.97)	2.50 (0.64)	2.79 (0.89)
Gd	5.22 (0.46)	4.78 (0.09)	6.78 (1.51)	4.51 (0.97)	7.97 (0.01)	6.57 (0.97)	7.40 (0.14)	5.07 (0.92)
Tb	0.55 (0.02)	0.43 (0.01)	0.90 (0.23)	0.59 (0.13)	1.15 (0.46)	1.05 (0.38)	1.09 (0.40)	0.98 (0.38)
Dy	3.13 (0.08)	2.55 (0.28)	4.93 (0.82)	3.66 (0.65)	5.68 (0.46)	4.63 (0.74)	5.03 (0.22)	3.83 (0.37)
Ho	1.18 (0.09)	0.79 (0.02)	0.81 (0.15)	0.41 (0.10)	0.98 (0.27)	0.97 (0.28)	1.12 (0.28)	0.83 (0.35)
Er	1.14 (0.13)	0.82 (0.16)	1.96 (0.31)	0.97 (0.34)	2.18 (0.71)	2.30 (0.69)	1.97 (0.44)	1.87 (0.46)
Tm	0.14 (0.02)	0.11 (0.07)	0.30 (0.04)	0.19 (0.03)	0.37 (0.15)	0.36 (0.13)	0.39 (0.11)	0.57 (0.24)
Yb	2.45 (0.20)	1.81 (0.21)	1.49 (0.36)	1.40 (0.36)	1.97 (0.42)	1.85 (0.84)	2.30 (1.04)	2.17 (0.75)
Lu	0.12 (0.01)	0.09 (0.01)	0.26 (0.04)	0.33 (0.04)	0.27 (0.12)	0.28 (0.04)	0.36 (0.13)	0.54 (0.26)
Hf	3.32 (0.66)	2.93 (0.02)	5.70 (0.89)	5.26 (0.05)	5.32 (0.73)	6.32 (0.99)	4.49 (0.04)	7.14 (1.26)
Ta	2.30 (0.56)	1.98 (0.18)	3.24 (0.23)	3.26 (0.48)	3.01 (0.41)	4.98 (0.86)	2.93 (0.78)	6.24 (0.67)
Pb	14.3 (1.6)	11.9 (0.4)	24.1 (2.0)	29.1 (2.8)	9.04 (0.76)	23.2 (2.8)	8.87 (1.43)	99.3 (6.1)
Th	3.82 (0.61)	3.08 (0.22)	9.26 (0.61)	9.24 (1.09)	2.58 (0.62)	7.01 (0.76)	1.71 (0.19)	12.9 (1.7)
U	1.42 (0.26)	1.29 (0.18)	2.74 (0.56)	2.82 (0.74)	1.08 (0.48)	2.49 (0.77)	0.82 (0.60)	5.22 (0.58)

RUN No.	10084-5		10084-6		10084-7	
n	Amp (5)	Gl (5)	Amp (5)	Gl (9)	Amp (4)	Gl (5)
Sc	25.7 (2.9)	4.32 (0.22)	21.6 (0.9)	4.51 (0.68)	19.1 (2.3)	3.78 (0.76)
Ti	20,776 (1390)	3954 (257)	16,039 (1896)	4540 (413)	34,230 (10,395)	12,456 (1255)
V	260 (24)	7.79 (1.06)	232 (20)	4.97 (0.84)	150 (10)	4.82 (0.30)
Cr	227 (23)	7.21 (1.07)	214 (15)	6.75 (0.39)	121 (15)	12.2 (1.4)
Rb	17.5 (1.2)	175 (7)	18.9 (1.5)	208 (7)	14.6 (1.6)	173 (3)
Sr	731 (68)	1495 (41)	731 (53)	1745 (66)	909 (46)	2154 (55)
Y	20.2 (2.0)	13.1 (1.6)	21.8 (1.3)	14.6 (1.4)	19.4 (1.9)	13.5 (1.8)
Zr	148 (12)	427 (10)	150 (17)	471 (16)	132 (12)	567 (37)
Nb	45.6 (2.8)	95.1 (2.5)	40.0 (4.3)	123 (6)	34.3 (2.8)	136 (9)
Cs	1.38 (0.90)	16.7 (0.3)	0.95 (0.56)	17.2 (0.9)	3.05 (0.47)	17.3 (1.1)
Ba	383 (26)	1369 (23)	418 (32)	1549 (58)	503 (25)	994 (191)
K	8962 (817)	34,957 (846)	9936 (1725)	32,476 (1521)	13,245 (1110)	34,304 (1518)
La	17.9 (1.4)	66.3 (3.9)	16.4 (2.1)	84.2 (4.0)	12.1 (1.3)	80.3 (4.2)

Table 3 continued

RUN No.	10084-5		10084-6		10084-7	
n	Amp (5)	Gl (5)	Amp (5)	Gl (9)	Amp (4)	Gl (5)
Ce	45.4 (4.6)	107 (25)	44.3 (1.2)	134 (25)	34.1 (1.4)	123 (28)
Pr	6.93 (1.33)	10.8 (1.5)	5.74 (0.25)	11.3 (1.1)	5.16 (0.54)	11.1 (1.1)
Nd	26.8 (2.8)	37.9 (1.2)	25.6 (2.9)	37.2 (1.1)	24.0 (1.7)	38.7 (11.7)
Sm	6.88 (0.25)	6.77 (0.45)	6.32 (0.70)	5.76 (0.68)	6.74 (0.27)	6.36 (0.79)
Eu	2.59 (0.38)	3.10 (0.72)	1.89 (0.52)	2.24 (0.39)	2.54 (0.25)	2.48 (0.74)
Gd	6.84 (0.39)	5.09 (0.11)	5.86 (0.27)	5.46 (0.54)	5.35 (0.44)	5.07 (0.09)
Tb	1.39 (0.41)	0.93 (0.24)	0.87 (0.20)	0.54 (0.18)	1.05 (0.24)	0.64 (0.22)
Dy	4.74 (0.86)	3.16 (0.37)	4.95 (0.83)	2.89 (0.90)	4.91 (0.33)	2.70 (0.67)
Ho	1.32 (0.52)	0.82 (0.31)	0.76 (0.14)	0.52 (0.22)	0.90 (0.33)	0.63 (0.13)
Er	2.31 (0.37)	1.66 (0.59)	1.82 (0.27)	1.29 (0.33)	1.88 (0.42)	1.42 (0.30)
Tm	0.43 (0.16)	0.47 (0.08)	0.26 (0.05)	0.28 (0.24)	0.38 (0.18)	0.29 (0.16)
Yb	2.29 (0.57)	2.07 (0.65)	1.20 (0.49)	0.93 (0.37)	2.25 (0.60)	1.35 (0.35)
Lu	0.51 (0.19)	0.47 (0.14)	0.19 (0.03)	0.30 (0.28)	0.31 (0.16)	0.22 (0.07)
Hf	4.46 (0.08)	7.81 (0.93)	3.76 (0.52)	7.94 (1.17)	3.18 (0.51)	10.1 (1.5)
Ta	2.64 (0.59)	7.59 (0.38)	2.31 (0.36)	8.91 (0.51)	1.55 (0.52)	9.08 (1.14)
Pb	10.2 (1.4)	107 (9)	9.05 (2.83)	123 (5)	6.63 (1.25)	145 (3)
Th	1.45 (0.77)	14.3 (0.9)	1.46 (0.42)	21.8 (1.3)	0.54 (0.26)	22.9 (1.9)
U	1.35 (0.79)	5.89 (0.87)	1.22 (0.83)	7.89 (0.65)	0.46 (0.17)	8.04 (0.36)

Trace element concentrations are reported in ppm (μg/g). *n* is the number of analyses. The numbers in the parentheses are standard deviation. For example, 20,776 (1390), 25.7 (2.9), and 4.32 (0.22) should be read as 20,776 ± 1390, 25.7 ± 2.9, and 4.32 ± 0.22, respectively

This study investigated the partitioning of trace elements between the crystalline amphibole and silicate liquid from the experimental products of crystallization of hydrous basalt melts at 0.6–2.6 GPa and 860–970 °C. A combination of electron microprobe (EMP) and laser ablation-inductively coupled plasma-mass spectrometry (LA-ICP-MS) was used to analyze major and trace elements in experimentally produced amphiboles and quenched glasses. The abundances of rare earth elements (REE), high-field strength elements (HFSE), large ion lithophile elements (LILE), actinides, and the transition metals in experimental phases were determined and the data were used to calculate the partition coefficients between amphiboles and glasses. In addition, the ideal radius, the maximum partition coefficient and the apparent Young's modulus of the M4 site of amphibole were estimated assuming that all REE^{3+} occupy this site.

2 Experimental strategy and analytical techniques

2.1 Starting material and experimental procedures

The starting material used in the crystallization experiments is a natural hydrous basalt (10,084) with modal mineralogy plagioclase (40%), iddingsitized olivine (25%), clinopyroxene (20%), matrix (10%) and minor iron titanium oxide (5%) from the Yichuan–Ruyang region in west Henan province, China. Table 1 shows the composition of the starting material (Zhou et al. 1998).

Two series of experiments (temperature series and pressure series) were conducted in the multi-anvil apparatus in the Key Laboratory for High Temperature and High Pressure Study of the Earth's Interior, Institute of Geochemistry, Chinese Academy of Sciences. Run conditions and the experimental protocol and configuration of charges for multi-anvil experiments were same with those described by Zhang et al. (2019). Fine-ground powder samples were loaded into 3 mm long graphite containers with inner diameter 4 mm, and placed between 1 mm thick graphite discs at each end. The pressure transmitting medium was pyrophyllite. In the "temperature series", charges were held at 0.6 GPa and 1460 °C for 1 h, then rapidly cooled isobarically to crystallization temperatures of 860 °C, 915 °C, or 970 °C, and held for 100 h before quenching. In the "pressure series", the charges were brought to superliquidus conditions (1460 °C and 0.6 GPa, 1490 °C and 1.1 GPa, 1515 °C and 1.6 GPa, 1540 °C and 2.1 GPa, or 1570 °C and 2.6 GPa) for 1 h, and then rapidly and isobarically cooled to an identical crystallization temperature of 970 °C and annealed for 100 h. All samples were quenched by shutting off the electric power. Experimental

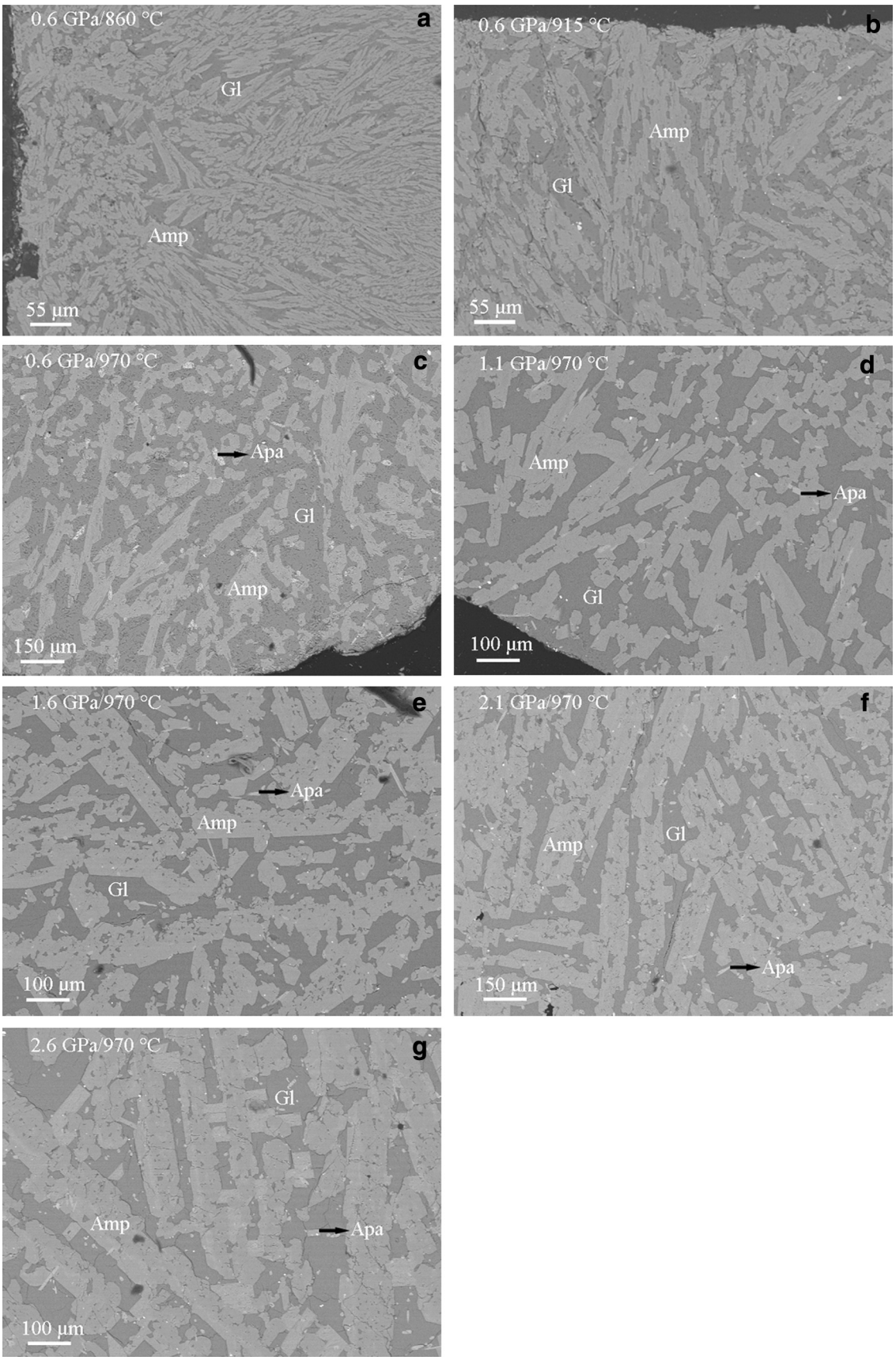
0.6 GPa/860 °C
a
Gl
Amp
55 μm
0.6 GPa/915 °C
b
Amp
Gl
55 μm
0.6 GPa/970 °C
c
Apa
Gl
Amp
150 μm
1.1 GPa/970 °C
d
Amp
Apa
Gl
100 μm
1.6 GPa/970 °C
e
Apa
Amp
Gl
100 μm
2.1 GPa/970 °C
f
Amp
Gl
Apa
150 μm
2.6 GPa/970 °C
g
Gl
Amp
Apa
100 μm

◀**Fig. 1** BSE images of experimental charges at 0.6–2.6 GPa and 860–970 °C illustrating coexisting minerals and glass and the increase in crystal size of amphibole with increasing pressure or temperature. *Amp* amphibole, *Apa* apatite, *Gl* glass

conditions are reported in Table 2. Run products were mounted in an epoxy disc and carefully polished for EMP and LA-ICP-MS analysis.

2.2 Analytical techniques

Major element compositions of phases were analyzed with the JEOL JXA-8100 electron microprobe at the Institute of Geology and Geophysics, Chinese Academy of Sciences. An accelerating voltage of 15 kV and beam current of 20 nA were employed. For mineral analysis, the beam diameter was 1–5 μm and a slightly defocused beam of 10 μm diameter was used for glass. Na and K were counted in the first pass to reduce the problem of Na and K loss during analyses (Morgan and London 2005). Major element compositions of amphibole and glass in the experimental products are reported in Table 2. Experimental charges were analyzed for trace elements by LA-ICP-MS (Agilent 7700X) at the State Key Laboratory of Ore Deposit Geochemistry, Institute of Geochemistry, Chinese Academy of Sciences. Laser sampling was performed using a Coherent GeolasPro laser ablation system (193 nm wavelength). Analytical methods are available in Huang et al. (2016). Each analysis incorporates an approximately 15 s background acquisition (gas blank) followed by 50 s data acquisition from the sample. Analytical spots (44 μm) were ablated by 160 successive laser pulses (4 Hz). Every 5–6 sample analyses were followed by one analysis of NIST SRM 610 in order to correct the time-dependent drift of sensitivity and mass discrimination. Data reduction was performed by *ICPMSDataCal* (Liu et al. 2008). Trace element compositions of amphibole and glass in the experimental products are summarized in Table 3.

3 Results

3.1 Description of run products

All of seven runs yielded amphibole-glass pairs that were suitable for the determination of trace element partition coefficients (Fig. 1, Table 2). The experimental phase assemblages are dominated by amphibole (Amp), glass (Gl). Some experiments also include accessory apatite (Apa), spinel (Sp), albite (Ab) or magnetite (Mt). Backscattered electron (BSE) images of the experimental charges illustrate the increasing crystal size of euhedral amphibole with increasing pressure or temperature. At 0.6 GPa and 860 °C, amphibole is about 80 μm in the maximum size and distributed within the glass (Fig. 1a). Amphibole-glass contacts are straight without any resorption textures. Furthermore, at 0.6 GPa and 970 °C, euhedral amphibole crystal of ~ 100 μm formed together with slightly smaller apatite (Fig. 1c). Amphibole crystal about 300 μm formed, which coexists with large, block apatite crystals at 2.6 GPa and 970 °C (Fig. 1g).

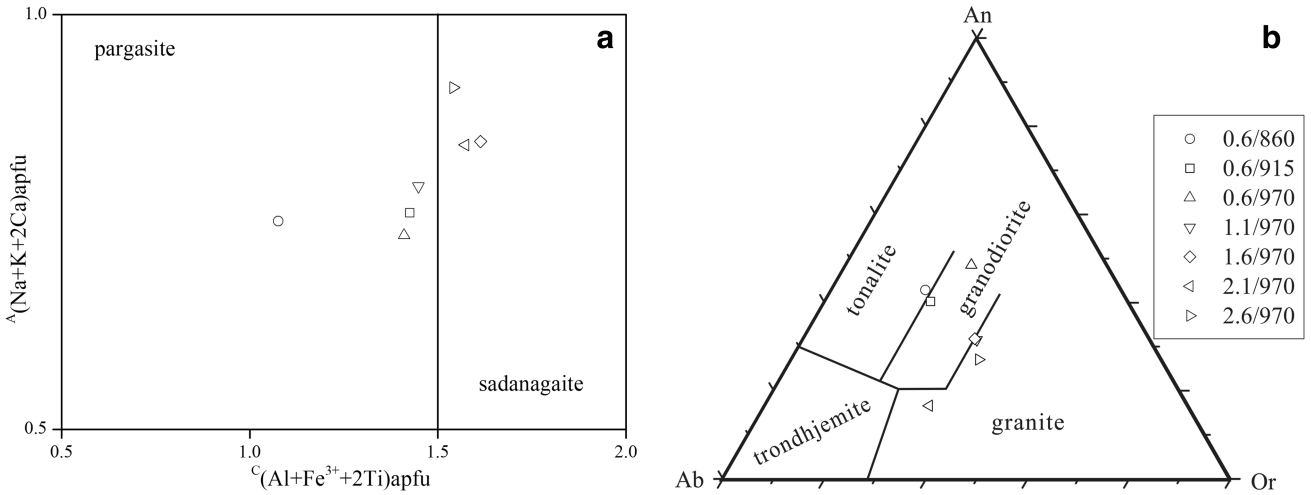

Fig. 2 Classifications of amphibole and glass in the experimental products. **a** Calcium amphibole and their compositional boundaries, showing the crystalline amphiboles at 0.6–1.1 GPa and 1.6–2.6 GPa fall in pargasite and sadanagaite fields, respectively. The calcium amphiboles defined by $^{B}(Ca + \Sigma M^{2+})/\Sigma B \geq 0.75$ and $^{B}Ca/\Sigma B \geq \Sigma M^{2+}/\Sigma B$. **b** CIPW normative An-Ab-Or plot for quenched glasses, showing the run liquids fall in tonalite and granodiorite fields at 0.6 GPa but fall in granodiorite to granite with increasing pressure. 0.6/860 means crystallization pressure *P* (GPa) and temperature *T* (°C) in the legend

3.2 Amphibole and glass compositions

Amphibole and glass have homogeneous major and trace element compositions in each run (Table 2, 3), and their classification is shown in Fig. 2. According to the recommendations of Hawthorne et al. (2012), all the experimental amphiboles belong to the calcic amphibole category and are classified pargasite/sadanagaite and have Mg# = 50–60 [Mg# = molar (100 × MgO/(MgO + FeO))]. Figure 2a shows the crystalline amphiboles at 0.6–1.1 GPa and 1.6–2.6 GPa fall in pargasite and sadanagaite fields, respectively. From the CIPW normative An-Ab-Or plot for quenched glasses, Fig. 2b shows the run liquids fall in tonalite and granodiorite fields at the lower pressure (0.6

Fig. 3 Trace elements partition coefficients (D_i) between amphiboles and glasses from this study and available literature studies. **a, b** Partition coefficients for REE; **c, d** Partition coefficients of high-field strength elements (Nb, Ta, Zr, Hf, Ti); **e, f** Partition coefficients of large ion lithophile elements K, Rb, Cs, Sr and Ba; **g, h** Partition coefficients for actinides (U, Th) and Pb; **i, j** Partition coefficients of transition metals (Sc, V, Cr). The legends of temperature series runs and the pressure series runs are shown in figure **a** and **b,** respectively. 0.6/860 means crystallization pressure P (GPa) and temperature T (°C) in the legend. *Open symbols* data from previous literature. 1.0/850, 900: Klein et al. (1997); 0.7/860, 890, 920, 950: Nandedkar et al. (2016); 1.25/900: Qian and Hermann (2013); 1.5/950: Wan et al. (2009) ▶

Table 4 Amphibole-glass partition coefficients

D	10084-1	10084-2	10084-3	10084-4	10084-5	10084-6	10084-7
Sc	1.11 (0.19)	1.13 (0.11)	1.85 (0.31)	6.49 (0.48)	5.96 (0.68)	4.80 (0.20)	5.07 (0.62)
Ti_m	1.08 (0.69)	1.18 (0.21)	1.82 (0.32)	4.22 (0.65)	5.25 (1.12)	3.53 (0.62)	2.75 (0.21)
V	1.06 (0.50)	1.16 (0.28)	2.26 (0.37)	30.08 (2.33)	33.43 (4.41)	46.67 (4.09)	31.15 (4.56)
Cr	1.05 (0.51)	1.45 (0.40)	1.82 (0.52)	12.36 (1.26)	31.59 (7.41)	31.72 (9.66)	9.94 (6.18)
Rb	1.06 (0.29)	0.85 (0.27)	0.35 (0.20)	0.11 (0.06)	0.10 (0.05)	0.09 (0.02)	0.08 (0.02)
Sr	1.36 (0.40)	0.99 (0.12)	0.79 (0.09)	0.55 (0.04)	0.49 (0.07)	0.42 (0.07)	0.42 (0.02)
Y	1.40 (0.41)	1.59 (0.24)	1.10 (0.18)	1.46 (0.28)	1.54 (0.15)	1.49 (0.09)	1.43 (0.15)
Zr	1.16 (0.50)	0.91 (0.15)	0.66 (0.12)	0.40 (0.03)	0.35 (0.03)	0.32 (0.04)	0.23 (0.02)
Nb	1.07 (0.66)	1.09 (0.12)	0.81 (0.11)	0.59 (0.05)	0.48 (0.07)	0.32 (0.03)	0.25 (0.02)
Cs	1.50 (0.77)	0.84 (0.33)	0.36 (0.22)	0.09 (0.07)	0.08 (0.05)	0.06 (0.03)	0.18 (0.20)
Ba	1.17 (0.35)	0.98 (0.17)	0.53 (0.13)	0.35 (0.07)	0.28 (0.06)	0.27 (0.06)	0.51 (0.03)
K_m	1.15 (0.12)	0.93 (0.11)	0.51 (0.06)	0.32 (0.03)	0.26 (0.06)	0.31 (0.09)	0.39 (0.10)
La	0.23 (0.02)	0.68 (0.25)	0.48 (0.27)	0.32 (0.19)	0.27 (0.13)	0.19 (0.03)	0.15 (0.02)
Ce	0.38 (0.04)	0.80 (0.27)	0.58 (0.28)	0.45 (0.22)	0.42 (0.14)	0.33 (0.05)	0.28 (0.04)
Pr	0.64 (0.07)	0.88 (0.26)	0.70 (0.28)	0.62 (0.25)	0.64 (0.22)	0.51 (0.11)	0.46 (0.09)
Nd	0.86 (0.13)	1.07 (0.31)	0.83 (0.30)	0.88 (0.28)	0.71 (0.13)	0.69 (0.08)	0.62 (0.12)
Sm	1.12 (0.41)	1.33 (0.41)	1.13 (0.21)	0.96 (0.29)	1.02 (0.33)	1.10 (0.12)	1.06 (0.20)
Eu	1.17 (0.36)	1.38 (0.30)	1.26 (0.32)	0.89 (0.23)	0.83 (0.12)	0.85 (0.23)	1.02 (0.10)
Gd	1.09 (0.42)	1.44 (0.27)	1.21 (0.31)	1.46 (0.42)	1.34 (0.08)	1.07 (0.23)	1.06 (0.28)
Tb	1.29 (0.46)	1.50 (0.29)	1.10 (0.44)	1.12 (0.41)	1.50 (0.44)	1.60 (0.36)	1.64 (0.37)
Dy	1.23 (0.22)	1.45 (0.29)	1.23 (0.32)	1.31 (0.32)	1.50 (0.27)	1.71 (0.29)	1.82 (0.12)
Ho	1.51 (0.97)	1.55 (0.26)	1.02 (0.28)	1.35 (0.34)	1.61 (0.63)	1.48 (0.28)	1.43 (0.52)
Er	1.38 (0.45)	1.66 (0.38)	0.95 (0.31)	1.05 (0.23)	1.40 (0.22)	1.41 (0.21)	1.32 (0.30)
Tm	1.35 (0.61)	1.59 (0.37)	1.03 (0.43)	0.68 (0.20)	0.91 (0.35)	0.93 (0.17)	1.28 (0.60)
Yb	1.36 (0.17)	1.06 (0.31)	1.07 (0.22)	1.06 (0.48)	1.11 (0.28)	1.28 (0.52)	1.67 (0.45)
Lu	1.30 (0.24)	0.90 (0.20)	0.97 (0.43)	0.67 (0.24)	1.08 (0.41)	0.64 (0.11)	1.38 (0.71)
Hf	1.14 (0.57)	1.08 (0.24)	0.84 (0.12)	0.63 (0.15)	0.57 (0.14)	0.47 (0.07)	0.32 (0.05)
Ta	1.16 (0.58)	0.99 (0.15)	0.60 (0.28)	0.47 (0.13)	0.35 (0.08)	0.26 (0.04)	0.17 (0.06)
Pb	1.20 (0.19)	0.83 (0.27)	0.39 (0.20)	0.09 (0.05)	0.10 (0.04)	0.07 (0.02)	0.05 (0.01)
Th	1.24 (0.22)	1.00 (0.28)	0.37 (0.23)	0.13 (0.09)	0.10 (0.05)	0.07 (0.02)	0.02 (0.01)
U	1.10 (0.33)	0.97 (0.29)	0.43 (0.19)	0.16 (0.11)	0.23 (0.13)	0.16 (0.03)	0.06 (0.02)

Uncertainties are the numbers in the parentheses and are reported as standard deviation with respect to the average and are calculated by propagating uncertainty of the individual phase. Ti_m, and K_m indicate partition coefficients based on microprobe measurements

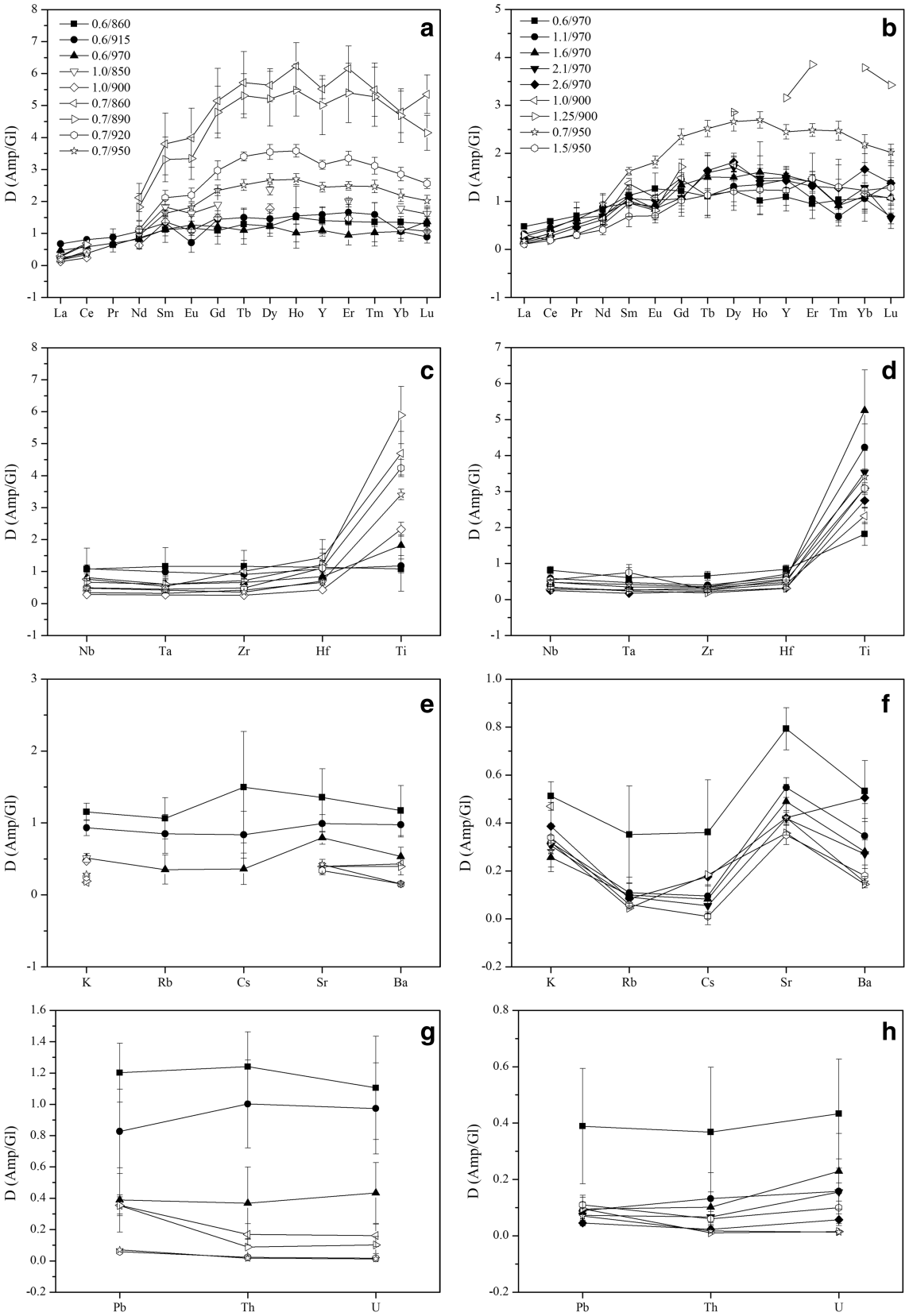
a
0.6/860
0.6/915
0.6/970
1.0/850
1.0/900
0.7/860
0.7/890
0.7/920
0.7/950
D (Amp/Gl)
La Ce Pr Nd Sm Eu Gd Tb Dy Ho Y Er Tm Yb Lu
b
0.6/970
1.1/970
1.6/970
2.1/970
2.6/970
1.0/900
1.25/900
0.7/950
1.5/950
D (Amp/Gl)
La Ce Pr Nd Sm Eu Gd Tb Dy Ho Y Er Tm Yb Lu
c
D (Amp/Gl)
Nb Ta Zr Hf Ti
d
D (Amp/Gl)
Nb Ta Zr Hf Ti
e
D (Amp/Gl)
K Rb Cs Sr Ba
f
D (Amp/Gl)
K Rb Cs Sr Ba
g
D (Amp/Gl)
Pb Th U
h
D (Amp/Gl)
Pb Th U

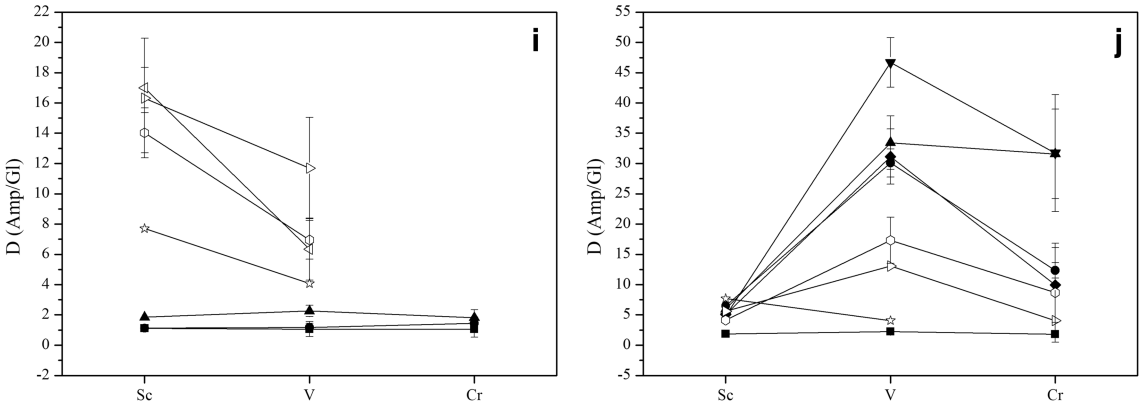

Fig. 3 continued

GPa) but in granodiorite to granite at the higher pressures (1.1–2.6 GPa). Most trace elements are present in smaller amounts in amphibole than those in coexisting glass, but the concentrations of medium to heavy rare earth elements of amphibole are greater than those in the glass (Table 3).

4 Discussion

4.1 Attainment of equilibrium

The attainment or close approach to thermodynamic equilibrium of crystallization during the experiment is an important prerequisite for accurate trace element partitioning coefficient. Although we did not perform reversal experiments, there are two arguments that suggest close approximation to equilibrium. Firstly, the experimental duration (100 h) of our study is longer than previous studies that have observed attainment of equilibrium (Klein et al. 1997; Klemme et al. 2002; Adam and Green 2006; Nandedkar et al. 2014). Secondly, the homogeneous composition of the quenched experimental products as indicated by the average standard deviations of less than $< 5\%$ for major elements (Table 2) and of less than $< 10\%$ for trace elements (Table 3) further support our interpretation that major and trace element equilibrium was achieved.

4.2 Trace element partitioning

Amphibole-glass partition coefficients (D_i) calculated from the average trace element concentrations are listed in Table 4 and summarized in Fig. 3. Uncertainties in the coefficients are estimated by error propagation from analytical uncertainties in the individual phase.

4.2.1 Rare earth elements

The amphibole–glass partition coefficients for REE in the temperature series products are illustrated in Fig. 3a. The light rare earth elements (LREE: La–Nd) are incompatible elements with the exception of Nd at 0.6 GPa and 915 °C. In contrast, medium to heavy rare earth elements (MREE-HREE: Sm–Lu) are compatible apart from Lu at 0.6 GPa and 915 °C, and Er and Lu at 0.6 GPa and 970 °C. This observation is consistent with the results from Nandedkar et al. (2016). The compatibility of HREE is slightly increasing with increasing atomic number except the Yb at 0.6 GPa and 915 °C. The behavior of Y is analogous to that of HREE due to its identical valence and similar cation radius. It is worthy note that the D_{REE} (with the exception of Yb and Lu) slightly increase at 915 °C and then decrease at 970 °C.

Moreover, most REE show a continuous, smooth change in their D values for amphibole-glass with increasing P in the pressure series products (Fig. 3b). All of the LREE are incompatible elements, and the D_{LREE} decrease with increasing pressure at isothermal 970 °C. But almost all of MREE and HREE are compatible elements apart from Sm at 1.1 GPa, Eu, Tm and Lu at 1.1 GPa to 2.1 GPa. Additionally, the most compatible rare earth element in the amphibole structure is dysprosium (Dy) in agreement with previous studies (Klein et al. 1997; Nandedkar et al. 2016).

Fig. 4 Onuma diagrams, log (D) versus cation radius, for REE▶ partition coefficients between amphibole and glass. Curves are fits of Eq. 1 to the data. Measuring these partition coefficients for REE show parabolic behavior. The REE^{3+} cations enter M4 site in amphibole from the temperature series products (**a**–**c**) and the pressure series products (**d**–**g**)

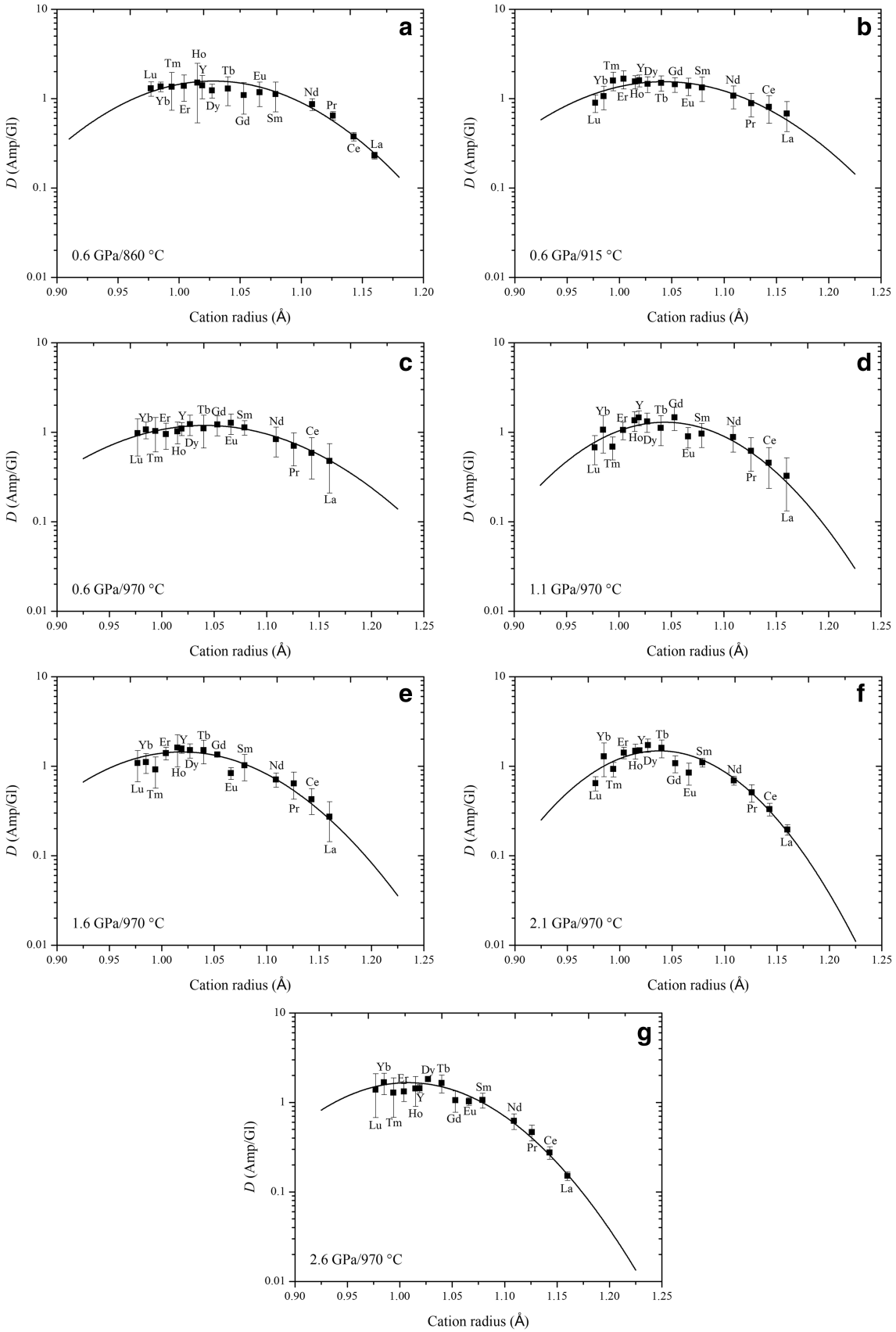
a
0.6 GPa/860 °C
b
0.6 GPa/915 °C
c
0.6 GPa/970 °C
d
1.1 GPa/970 °C
e
1.6 GPa/970 °C
f
2.1 GPa/970 °C
g
2.6 GPa/970 °C
D (Amp/Gl)
Cation radius (Å)

The partition coefficients for some MREE (Eu, Tb, and Dy) and HREE (Tm and Yb) are positively proportional to pressure at 0.6–2.6 GPa and 970 °C.

4.2.2 High-field strength elements

HFSE are tetra- or penta-valent cations such as Nb, Ta, Zr, Hf, and Ti. The amphibole–glass partition coefficients for HFSE in the temperature series products are plotted in Fig. 3c. The partition coefficients of HFSE are > 1 at 0.6 GPa and 860 °C. But the HFSE become weakly compatible with incompatible as the temperature increases from 860 to 970 °C at 0.6 GPa, with the exception of Ti, which is compatible in the amphibole, as also shown in previous studies (Tiepolo et al. 2007; Nandedkar et al. 2016).

Nb, Ta, Zr, and Hf are incompatible and their partition coefficients are generally < 1 in the pressure series, but the D_{Ti} is greater than one (Fig. 3d). In addition, the HFSE (with the exception of Ti) partition coefficients tend to decrease as the pressure increases from 0.6 to 2.6 GPa at 970 °C. In summary, the partition coefficients for HFSE increase with decreasing temperature or pressure, and the Ti is more compatible than other HFSE.

4.2.3 Large ion lithophile elements

Besides the result of 0.6 GPa and 860 °C, the LILE are incompatible elements with partition coefficients generally below 1 in the temperature series and the pressure series (Fig. 3e, f). In the temperature series products, the LILE are weakly compatible with moderately incompatible with increasing temperature at 0.6 GPa. The partition coefficient of the potassium (K) in this study indicates the same trend relative to Klein et al. (1997) and decreases with increasing temperature, but Nandedkar et al. (2016) show an opposite trend. In the pressure series products, the partition coefficients for most LILE exhibit a negative correlation with pressure at 0.6–2.6 GPa and 970 °C. Moreover, D_{LILE} from the pressure series experiments show a uniform pattern when plotted against the atomic number in agreement with previous studies (Wan et al. 2009; Nandedkar et al. 2016), with the exception of Cs, Sr, and Ba in the run of 2.6 GPa and 970 °C and Cs, Sr in the study of Qian and Hermann (2013). Another similarity is the maximum partition coefficient for Sr except for Ba at 2.6 GPa and 970 °C.

4.2.4 Actinides

Uranium (U) and thorium (Th) amphibole–glass partition coefficients are reported in Fig. 3g, h together with the partition coefficient for Pb. Besides the result of 0.6 GPa and 860 °C, the actinides elements are incompatible

Table 5 Fitting parameters used in the lattice strain model for REE^{3+} cations in amphibole

P/GPa	*T*/°C	r_0/Å	σ	D_0	σ	*E*/GPa	σ	Melt composition	References
0.6	860	1.01	0.01	1.38	0.1	142	31	Tonalite	This study
0.6	915	1.04	0.03	1.52	0.1	162	26	Granodiorite	
0.6	970	1.04	0.01	1.18	0.08	165	41	Tonalite	
1.1	970	1.04	0.02	1.26	0.1	273	56	Granodiorite	
1.6	970	1.03	0.03	1.41	0.09	271	22	Granite	
2.1	970	1.03	0.04	1.44	0.1	370	69	Granite	
2.6	970	1.01	0.01	1.52	0.1	238	25	Granite	
1.0	900	1.03	0.007	1.7	0.8	110	80	Andesite	Green and Pearson (1985)
1.5	1000	0.99	0.03	1.3	0.2	204	81	Andesite	Brenan et al. (1995)
1.5	1150	1.03	–	0.6	–	390	–	Basanite	LaTourrette et al. (1995)
1.0	800	1.03	0.01	2.66	0.19	170	60	Tonalite	Klein et al. (1997)
1.0	850	1.03	0.01	2.29	0.1	250	60		
1.0	900	1.03	0.01	1.75	0.1	300	80		
1.0	1025	1.035	–	0.64	–	300	–	Basanite	Adam and Green (2006)
2.0	1050	1.03	–	0.41	–	320	–		
1.5	950	0.995	0.006	1.32	0.03	233	35	Granodiorite	Wan et al. (2009)
0.7	950	1.02	0.001	2.63	0.03	339	9	Andesite	Nandedkar et al. (2016)

σ indicates 1 sigma standard deviation of these fitting parameters. (–) no value available

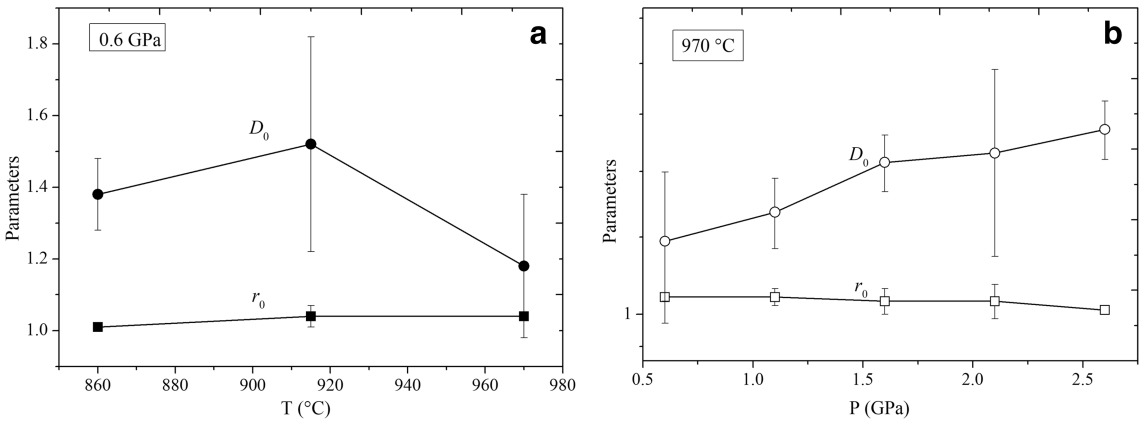

Fig. 5 Change of fitting parameters r_0, D_0 of the REE with increasing T at isobaric 0.6 GPa (**a**), and increasing P at isothermal 970 °C (**b**)

elements with partition coefficients below 1 in the temperature series and the pressure series. Th and U show decreasing partition coefficients with increasing temperature with D_{Th} varying from 1.24 to 0.37 and D_U from 1.1 to 0.43. Similar to temperature series, U and Th show a consistent decrease in partition coefficients between 0.6 and 2.6 GPa. D_{Pb} displays a decrease with increasing temperature or pressure. However, our data show substantially higher partition coefficients for actinides than that in previous studies (Klein et al. 1997; Nandedkar et al. 2016). Probably, the result has to do with the relatively lower silica concentration of glasses from this experiment.

4.2.5 Transition metals

The partition coefficients for transition metals are rarely reported in the literature. Three transition metals, Sc, V and Cr, are investigated in this study (Fig. 3i, j); all of them are compatible elements and their partition coefficients positively correlate with temperature, with D_{Sc}, D_V, and D_{Cr} ranging from 1.11 to 1.85, 1.06 to 2.26, and 1.05 to 1.82 at 860–970 °C, respectively. Similarly, their partition coefficients trend to increase with increasing pressure. For V and Cr, there is a notable increase in partition coefficients between 0.6 and 1.1 GPa. Nandedkar et al. (2016) suggested the substantial increase of D for transition metals is related to change of the melt structure.

4.3 D_{REE}^{Amp-Gl} with the lattice strain model

The influence of cation radius (Shannon 1976) on partitioning behavior for trace elements has been described by many publications (Onuma et al. 1968; Brice 1975; Blundy and Wood 1994; Wood and Blundy 1997; Blundy and Wood 2003). The relationship, Lattice Strain Model-LSM,

$$D_i = D_0 \exp \frac{-4\pi E N_A \left[\frac{r_0}{2}(r_i - r_0)^2 + \frac{1}{3}(r_i - r_0)^3\right]}{RT} \quad (1)$$

relates the Nernst partition coefficients of elements i (D_i) for isovalent cations in crystals and melts as a function of cation radius (r_i), the strain-free partition coefficient (D_0) that has an ionic radius r_0 equal to the strain-free lattice size of the crystallographic site, and an elastic constant E (apparent Young's modulus) that is specific to the host cation site. N_A is Avogadro's constant, R is the universal gas constant, and T is temperature in Kelvin.

According to the lattice strain model, the r_0, D_0, and E are estimated by combining with the partition coefficients of trivalent REE between amphiboles and silicate glasses. Partition coefficients versus cation radius for the REE^{3+} cations entering M4 site of amphibole are plotted in Fig. 4, these Onuma diagrams display the parabolic shape. A set of parabolas have the following ranges in fitting parameter values for the M4 site of amphibole, r_0 1.01–1.04 Å, D_0 1.18–1.38, and E 142–165 GPa at 0.6 GPa and 860–970 °C (Fig. 4a–c, Table 5). Although some previous studies suggested that the D_0 decreases with increasing temperature (Klein et al. 1997; Nandedkar et al. 2016; Shimizu et al. 2017), our D_0 has the maximum value at 0.6 GPa and 915 °C rather than at 860 °C (Fig. 5a). Nevertheless, the D_0 trends to decrease at the range of 860–970 °C. Furthermore, Shimizu et al. (2017) verified that D_0 positively correlates with the silica content of the coexisting glass. The maximum REE partition coefficient D_0 corresponds with the highest silica content of the coexisting glass at 0.6 GPa and 915 °C. For example, the REE are easier enriched in amphibole if the quenched glass is granodiorite or granite in this study, and the D_0 values are similar to the result of Wan et al. (2009). However, the D_0 between amphibole and tonalitic glass (Klein et al. 1997) and between amphibole and andesitic glass (Green

and Pearson, 1985; Brenan et al. 1995; Nandedkar et al. 2016) are greater compared to amphibole-basaltic glass pair (LaTourrette et al. 1995; Adam and Green 2006). Thus, glass composition exerts the dominant control on the incorporation of REE on the M4 site of amphibole at 0.6 GPa and 860–970 °C.

In addition, the fitting parameters are r_0 1.01–1.04 Å, D_0 1.18–1.52, and E 165–370 GPa at 0.6–2.6 GPa and 970 °C (Fig. 4c–g, Table 5). Amphibole-glass REE partition coefficients have been shown to negatively correlate with P in some previous studies (Adam and Green 1994, 2003; Dalpé and Baker 2000), but our D_0 increases with increasing pressure (Fig. 5b). In the 'melt model' from Shimizu et al. (2017), the D_0 negatively correlates with Ti and Ca contents in the glass, and the pressure series shows the same result in this study. Thus, the effect of pressure is significant for the partition coefficient of REE between amphibole and coexisting glass at 0.6–2.6 GPa and 970 °C. The ideal radius r_0 of amphibole M4 is almost constant both temperature series and pressure series, and the E trends to increase with increasing temperature or pressure (with the exception of 2.6 GPa).

5 Conclusions

The calcic amphibole is a sufficiently dominant mineral phase from crystallization of hydrous basalt melts at 0.6–2.6 GPa and 860–970 °C, and the coexisting glass compositions are tonalite, granodiorite, and granite.

The LREE are dominantly distributed in the glass rather than the amphibole in this study. In contrast, most MREE and HREE are compatible in amphibole. These patterns are in good agreement with previous findings, with the REE becoming increasingly compatible with decreasing ionic radius (Klein et al. 1997; Wan et al. 2009; Nandedkar et al. 2016). It is notable that at 0.6 GPa, the D_{REE} (with the exception of Yb and Lu) slightly increase at 915 °C but then decrease at 970 °C. Similarly, the D_0^{M4} for REE increases at 915 °C and then decreases at 970 °C. However, the D_0^{M4} values positively correlate with the pressure for REE in the amphibole-glass pairs. Furthermore, the derived best-fit values for r_0^{M4} and E^{M4} are almost constant and trend to increase with rising temperature or pressure, respectively. Although the LILE, HFSE (except the Ti), and actinides show a continuous decrease in compatibility with increasing temperature or pressure, the D of transition metals is inversely proportional to the T-P conditions in these experimental series. The experimental observations strongly suggest that the melt compositions play an important role to control the partition coefficient between amphibole and glass. The REE become more enriched in amphibole if the quenched glass is granodiorite or granite compared to the tonalitic glasses.

Acknowledgements We wish to thank Ms. Zhihui Dai for her assistance during LA-ICP-MS analyses. This work benefited from the financial support of the National Natural Science Foundation of China (Grant Nos. 41274105 and 41772043), the Joint Research Fund in Huge Scientific Equipment (U1632112) under cooperative agreement between NSFC and CAS, the Chinese Academy of Sciences "Light of West China" Program (Dawei Fan, 2017), Youth Innovation Promotion Association CAS (Dawei Fan, 2018), the Strategic Priority Research Program (B) of the Chinese Academy of Sciences (XDB 18010401), the CPSF-CAS Joint Foundation for Excellent Postdoctoral Fellows (Grant No. 2017LH014), and China Postdoctoral Science Foundation (Grant No. 2018M631104), the Guizhou Provincial Science and Technology Foundation (20171078), and the Guizhou Institute of Technology Foundation (XJGC20130901).

References

Adam J, Green TH (1994) The effects of pressure and temperature on the partitioning of Ti, Sr and REE between amphibole, clinopyroxene and basanitic melts. Chem Geol 117(1):219–233

Adam J, Green T (2006) Trace element partitioning between mica- and amphibole-bearing garnet lherzolite and hydrous basanitic melt: 1. Experimental results and the investigation of controls on partitioning behaviour. Contrib Mineral Petrol 152(1):1–17

Arzamastsev AA, Arzamastseva LV, Bea F, Montero P (2009) Trace elements in minerals as indicators of the evolution of alkaline ultrabasic dike series: LA-ICP-MS data for the magmatic provinces of northeastern Fennoscandia and Germany. Petrol 17(1):46–72

Blundy J, Dalton J (2000) Experimental comparison of trace element partitioning between clinopyroxene and melt in carbonate and silicate systems, and implications for mantle metasomatism. Contrib Mineral Petrol 139(3):356–371

Blundy J, Wood B (1994) Prediction of crystal-melt partition coefficients from elastic moduli. Lett Nat 372:452–454

Blundy J, Wood B (2003) Partitioning of trace elements between crystals and melts. Earth Planet Sci Lett 210(3–4):383–397

Brenan JM, Shaw HF, Ryerson FJ, Phinney DL (1995) Experimental determination of trace-element partitioning between pargasite and a synthetic hydrous andesitic melt. Earth Planet Sci Lett 135:1–11

Brice J (1975) Some thermodynamic aspects of the growth of strained crystals. J Cryst Growth 28(2):249–253

Chang CY, Li FB, Liu CS, Gao JF, Tong H, Chen MJ (2016) Fractionation characteristics of rare earth elements (REEs) linked with secondary Fe, Mn, and Al minerals in soils. Acta Geochim 35(4):329–339

Cui LF, Zhao ZQ, Liu CQ, Xu S, Liu TZ, Tu CL, Ding H (2017) Behavior of rare earth elements in granitic profiles, eastern Tibetan Plateau, China. Acta Geochim 36(3):552–555

Dalpé C, Baker DR (2000) Experimental investigation of large-ion-lithophile-element-, high-field-strength-element- and rare-earth-element-partitioning between calcic amphibole and basaltic melt: the effects of pressure and oxygen fugacity. Contrib Mineral Petrol 140(2):233–250

Dasgupta R, Hirschmann MM, McDonough WF, Spiegelman M, Withers AC (2009) Trace element partitioning between garnet lherzolite and carbonatite at 6.6 and 8.6 GPa with applications to the geochemistry of the mantle and of mantle-derived melts. Chem Geol 262(1–2):57–77

Draper DS, Westrenen W (2007) Quantifying garnet-melt trace element partitioning using lattice-strain theory: assessment of statistically significant controls and a new predictive model. Contrib Mineral Petrol 154(6):731–746

Frei D, Liebscher A, Franz G, Wunder B, Klemme S, Blundy J (2009) Trace element partitioning between orthopyroxene and anhydrous silicate melt on the lherzolite solidus from 1.1 to 3.2 GPa and 1230 to 1535°C in the model system Na_2O–CaO–MgO–Al_2O_3–SiO_2. Contrib Mineral Petrol 157(4):473–490

Green TH, Pearson NJ (1985) Rare earth partitioning between clinopyroxene and silicate liquid at moderate to high pressure. Contrib Mineral Petrol 74:201–216

Hawthorne FC, Oberti R, Martin RF, Harlow GE, Maresch WV, Schumacher JC, Welch MD (2012) Nomenclature of the amphibole supergroup. Am Miner 97:2031–2048

Hill E, Blundy JD, Wood BJ (2011) Clinopyroxene–melt trace element partitioning and the development of a predictive model for HFSE and Sc. Contrib Mineral Petrol 161(3):423–438

Huang XW, Gao JF, Qi L, Meng YM, Wang YC, Dai ZH (2016) In-situ LA–ICP–MS trace elements analysis of magnetite: the Fenghuangshan Cu–Fe–Au deposit, Tongling, Eastern China. Ore Geol Rev 72:746–759

Klein M, Stosch HG, Seck HA (1997) Partitioning of high field-strength and rare-earth elements between amphibole and quartz-dioritic to tonalitic melts: an experimental study. Chem Geol 138(3):257–271

Klemme S, Dalpé C (2003) Trace-element partitioning between apatite and carbonatite melt. Am Mineral 88(4):639–646

Klemme S, Blundy JD, Wood BJ (2002) Experimental constraints on major and trace element partitioning during partial melting of eclogite. Geochim Cosmochim Acta 66(17):3109–3123

Klemme S, Prowatke S, Hametner K, Günther D (2005) Partitioning of trace elements between rutile and silicate melts: implications for subduction zones. Geochim Cosmochim Acta 69(9):2361–2371

Landwehr D, Blundy J, Chamorro-Perez EM, Hill E, Wood B (2001) U-series disequilibria generated by partial melting of spinel lherzolite. Earth Planet Sci Lett 188(3):329–348

LaTourrette T, Hervig RL, Holloway JR (1995) Trace element partitioning between amphibole, phlogopite, and basanite melt. Earth Planet Sci Lett 135(1):13–30

Liu Y, Hu Z, Gao S, Gunther D, Xu J, Gao C, Chen H (2008) *In-situ* analysis of major and trace elements of anhydrous minerals by LA-ICP-MS without applying an internal standard. Chem Geol 257(1–2):34–43

Lundstrom C, Gill J, Williams Q (2000) A geochemically consistent hypothesis for MORB generation. Chem Geol 162(2):105–126

Mollo S, Blundy J, Giacomoni P, Nazzari M, Scarlato P, Coltorti M, Langone A, Andronico D (2017) Clinopyroxene-melt element partitioning during interaction between trachybasaltic magma and siliceous crust: clues from quartzite enclaves at Mt. Etna volcano. Lithos 284:447–461

Morgan GB, London D (2005) Effect of current density on the electron microprobe analysis of alkali aluminosilicate glasses. Am Mineral 90:1131–1138

Nandedkar RH, Ulmer P, Müntener O (2014) Fractional crystallization of primitive hydrous arc magmas: an experimental study at 0.7 GPa. Contrib Mineral Petrol 167(6):1015

Nandedkar RH, Hürlimann N, Ulmer P, Müntener O (2016) Amphibole–melt trace element partitioning of fractionating calc-alkaline magmas in the lower crust: an experimental study. Contrib Mineral Petrol 171(8–9):1–25

Nardi LVS, Formoso MLL, Müller IF, Fontana E, Jarvis K, Lamarão C (2013) Zircon/rock partition coefficients of REEs, Y, Th, U, Nb, and Ta in granitic rocks: uses for provenance and mineral exploration purposes. Chem Geol 335:1–7

Olin PH, Wolff JA (2010) Rare earth and high field strength element partitioning between iron-rich clinopyroxenes and felsic liquids. Contrib Mineral Petrol 160(5):761–775

Onuma N, Higuchi H, Wakita H, Nagasawa H (1968) Trace element partition between two pyroxenes and the host lava. Earth Planet Sci Lett 5:47–51

Parker MVK, Liebscher A, Frei D, Sijl JV, Westrenen WV, Blundy J, Franz G (2010) Experimental and computational study of trace element distribution between orthopyroxene and anhydrous silicate melt: substitution mechanisms and the effect of iron. Contrib Mineral Petrol 159(4):459–473

Prowatke S, Klemme S (2006) Trace element partitioning between apatite and silicate melts. Geochim Cosmochim Acta 70(17):4513–4527

Qian Q, Hermann J (2013) Partial melting of lower crust at 10–15 kbar: constraints on adakite and TTG formation. Contrib Mineral Petrol 165(6):1195–1224

Severs MJ, Beard JS, Fedele L, Hanchar JM, Mutchler SR, Bodnar RJ (2009) Partitioning behavior of trace elements between dacitic melt and plagioclase, orthopyroxene, and clinopyroxene based on laser ablation ICPMS analysis of silicate melt inclusions. Geochim Cosmochim Acta 73(7):2123–2141

Shannon RD (1976) Revised effective ionic radii and systematic studies of interatomic distances in halides and chalcogenides. Acta Cryst A32:17

Shimizu K, Liang Y, Sun C, Jackson CR, Saal AE (2017) Parameterized lattice strain models for REE partitioning between amphibole and silicate melt. Am Mineral 102:2254–2267

Stead CV, Tomlinson EL, McKenna CA, Kamber BS (2017) Rare earth element partitioning and subsolidus exchange behaviour in olivine. Chem Geol 475:1–13

Sun C (2018) Partitioning and partition coefficients. In: White W (ed) Encyclopedia of geochemistry. Encyclopedia of earth sciences series. Springer, Cham

Sun C, Liang Y (2012) Distribution of REE between clinopyroxene and basaltic melt along a mantle adiabat: effects of major element composition water and temperature. Contrib Mineral Petrol 163:807–823

Sun C, Liang Y (2013a) Distribution of REE and HFSE between low-Ca pyroxene and lunar picritic melts around multiple saturation points. Geochim Cosmochim Acta 119:340–358

Sun C, Liang Y (2013b) The importance of crystal chemistry on REE partitioning between mantle minerals (garnet clinopyroxene orthopyroxene and olivine) and basaltic melts. Chem Geol 358:23–36

Sun C, Graff M, Liang Y (2017) Trace element partitioning between plagioclase and silicate melt: the importance of temperature and plagioclase composition, with implications for terrestrial and lunar magmatism. Geochim Cosmochim Acta 206:273–295

Sweeney R, Green D, Sie S (1992) Trace and minor element partitioning between garnet and amphibole and carbonatitic melt. Earth Planet Sci Lett 113(1–2):1–14

Sweeney RJ, Prozesky V, Przybylowicz W (1995) Selected trace and minor element partitioning between peridotite minerals and carbonatite melts at 18–46 kb pressure. Geochim Cosmochim Acta 59(18):3671–3683

Thomas J, Bodnar R, Shimizu N, Sinha A (2002) Determination of zircon/melt trace element partition coefficients from SIMS analysis of melt inclusions in zircon. Geochim Cosmochim Acta 66(16):2887–2901

Tiepolo M, Vannucci R, Bottazzi P, Oberti R, Zanetti A, Foley SF (2000) Partitioning of REE, Y, Th, U and Pb between pargasite, kaersutite and basante to trachite melts: implications for percolated and veined mantle. Geochem Geophys Geosyst 1:2000GC000064

Tiepolo M, Oberti R, Zanetti A, Vannucci R, Foley SF (2007) Trace-element partitioning between amphibole and silicate melt. Rev Mineral Geochem 67(1):417–452

Wan F, Zhou W, Jiang N, Fan D, Chen H, Xie H (2009) The partition characteristic of trace elements in the partial melting massive amphibolite at 1.5 Gpa and 950 °C. Earth Sci Front 16(1):125–133

Westrenen WV, Draper DS (2007) Quantifying garnet-melt trace element partitioning using lattice-strain theory: new crystal-chemical and thermodynamic constraints. Contrib Mineral Petrol 154(6):717–730

Wood BJ, Blundy JD (1997) A predictive model for rare earth element partitioning between clinopyroxene and anhydrous silicate melt. Contrib Mineral Petrol 129:166–181

Xiong X, Adam J, Green T (2005) Rutile stability and rutile/melt HFSE partitioning during partial melting of hydrous basalt: implications for TTG genesis. Chem Geol 218(3–4):339–359

Zajacz Z, Halter W (2007) LA-ICPMS analyses of silicate melt inclusions in co-precipitated minerals: quantification, data analysis and mineral/melt partitioning. Geochim Cosmochim Acta 71(4):1021–1040

Zhang B, Hu XX, Asimow PD, Zhang X, Xu JG, Fan DW, Zhou WG (2019) Crystal size distribution of amphibole grown from hydrous basaltic melt at 0.6–2.6 GPa and 860–970 °C. Am Miner. https://doi.org/10.2138/am-2019-6759

Zhou WG, Zhang BR, Zhao ZD, Xie HS (1998) Geochemical characteristics and the provenance of cenozoic basic volcanic rocks in western Henan province, China. J Miner Pet 18:51–57 **(In Chinese with English abstract)**